Available online at www.sciencedirect.com

ScienceDirect

Procedia IUTAM 26 (2018) 132–144

Procedia IUTAM

www.elsevier.com/locate/procedia

IUTAM Symposium Wind Waves, 4-8 September 2017, London, UK

Comparison of Different Models for Wave Generation of The Hasselmann Equation

Andrei Pushkarev[a,b,c,*]

[a]Lebedev Physical Institute RAS, Leninsky 53, Moscow 119991, Russia
[b]Novosibirsk State University, Pirogova 1, Novosibirsk 630090, Russia
[c]Waves and Solitons LLC, 1719 W. Marlette Ave., Phoenix, AZ 85015, USA

Abstract

We compare two recently developed sets of source terms, based on different assumptions of wave energy input and dissipation, for Hasselmann equation. The numerical simulation, performed for limited fetch conditions with the constant wind speed shows the difference in total energy and mean frequency distributions along the fetch as well as in wave energy spectra. Possible reasons of such deviations are offered.

Peer-review under responsibility of the scientific committee of the IUTAM Symposium Wind Waves.

Keywords:
Hasselmann equation; wind and dissipation source terms; self-similar solutions; Kolmogorov-Zakharov spectra; wave-breaking dissipation; magic relation

1. Introduction

The physical oceanography community consents on the fact [5] that deep water ocean gravity surface wave forecasting models are described by Hasselmann equation (hearafter HE) [10, 11], also known as kinetic equation for waves, or energy balance equation:

$$\frac{\partial \varepsilon}{\partial t} + \frac{\partial \omega_k}{\partial \vec{k}} \frac{\partial \varepsilon}{\partial \vec{r}} = S_{nl} + S_{in} + S_{diss} \tag{1}$$

where $\varepsilon = \varepsilon(\omega_k, \theta, \vec{r}, t)$ is the wave energy spectral density, as the function of wave frequency $\omega_k = \omega(k)$, angle θ, two-dimensional real space coordinate $\vec{r} = (x, y)$ and time t. S_{nl}, S_{in} and S_{diss} are the nonlinear, wind input and wave-breaking dissipation source terms, respectively. Hereafter, only the deep water case, $\omega = \sqrt{gk}$ is considered, where g is the gravity acceleration and $k = |\vec{k}|$ is the absolute value of the vector wavenumber $\vec{k} = (k_x, k_y)$.

* Corresponding author.
E-mail address: dr.push@gmail.com

2210-9838
Peer-review under responsibility of the scientific committee of the IUTAM Symposium Wind Waves.
10.1016/j.piutam.2018.03.013

Since Hasselmann work, Eq.(1) has become the basis of operational wave forecasting models such as WAM, SWAN and Wavewatch III [24, 22]. While the physical oceanography community consents on the general applicability of Eq.(1), there is no consensus agreement on universal parameterizations of the source terms S_{nl}, S_{in} and S_{diss}.

Two different forms of S_{nl} term have been derived independently from the Euler equations for free surface incompressible potential flow of a liquid by [10, 11] and [30]. Their identity on the resonant surface

$$\omega_{\vec{k_1}} + \omega_{\vec{k_2}} = \omega_{\vec{k_3}} + \omega_{\vec{k_4}} \tag{2}$$

$$\vec{k_1} + \vec{k_2} = \vec{k_3} + \vec{k_4} \tag{3}$$

has been shown in [21].

S_{nl} term is the complex nonlinear operator acting on ε_k, concealing hidden symmetries [31, 33]. The most robust, first approximation of HE

$$S_{nl} = 0 \tag{4}$$

plays the crucial role in the weak turbulent theory [33] due to leading role of the S_{nl} source term in HE [28, 29]. Its simplest solution

$$\varepsilon \simeq \frac{P^{1/3}}{\omega^4} \simeq \beta g \frac{P^{1/3}}{\omega^4} \simeq \frac{\beta g U_*}{\omega^4} \simeq \frac{2\pi\alpha g U_{\lambda/2}}{\omega^4} \tag{5}$$

where P is the energy flux toward high wave numbers, β is small dimensionless parameter (the "Toba constant" [23]), g is the gravity acceleration, U_* is the wind friction velocity, $U_{\lambda/2}$ is the wind velocity at the height of half wavelength of the wave-number, corresponding to the spectral peak, and $\alpha = 0.00553$ [19]. Eq.(5) is known as Zakharov-Filonenko solution of HE [30], which is the subset of Kolmogorov-Zakharov (hearafter KZ) solutions .

The accuracy advantage of knowing the analytical expression for the S_{nl} term, also known in physical oceanography as XNL, is overshadowed by its computational complexity. Today, none of the operational wave forecasting models can afford to perform XNL computations in real time. Instead, their low computational capacity operational approximations, known as DIA and its derivatives, are used as its surrogates. The implication of such simplification is the inclusion of a tuning coefficient in front of nonlinear term; however, several publications have shown that DIA does not provide a good approximation of the actual XNL form. The paradigm of replacement of the XNL by the DIA and its variations leads to even more grave consequences: other source terms must be adjusted to allow the model Eq.(1) to produce desirable results. In other words, deformations suffered by XNL model due to the replacement of S_{nl} by its surrogates, need to be compensated by non-physical modification of other source terms to achieve reasonable model behavior in any specific case, leading to a loss of physical universality in HE model.

In contrast to S_{nl}, the knowledge of S_{in} and S_{diss} source terms is poor; furthermore, both include many heuristic factors and coefficients. The creation of a reliable, well justified theory of S_{in} has been hindered by strong turbulent fluctuations, uncorrelated with the wave motions, in boundary layer over the sea surface. Even one of the most crucial elements of this theory, the vertical distribution of horizontal wind velocity in the region closest to the ocean surface, where wave motions strongly interact with atmospheric motions, is still the subject of debates. The history of the development of different wind input forms is full of heuristic assumptions, which fundamentally restrict the magnitude and directional distribution of this term. As a result, the values of different wind input terms scatter by a factor of $300 - 500\%$ [2, 17]. For example, experimental determination of S_{in}, as provided by direct measurements of the momentum flux from the air to the water, cannot be rigorously performed in a laboratory due to gravity waves dispersion dependence on the water depth, as well as the problems with scale effects for laboratory winds. The good demonstration of the fact has been presented by [9]. Additional information on the detailed analysis of current state of the art of wind input terms can be found in [17].

Similar to the wind input term, there is little consent on the parameterization of the dissipation source term S_{diss}. The physical dissipation mechanism, which most physical oceanographers agree on, is the effect of wave energy loss due to wave breaking, while there are also other dubious ad-hoc "long wave" dissipation source terms, having heuristically justified physical explanations. Currently, there is no even an agreement on the location of wave breaking events in Fourier space. The approach currently utilized in operational wave forecasting models mostly relies on the dissipation, localized in the vicinity of the spectral energy peak. Recent numerical experiments [17, 8, 32] show,

however, that such approach does not pass most of the tests associated with the essentially nonlinear nature of the HE Eq.(1).

As the result of the above mentioned problems, WAVEWATCH operational model [24] has more than two dozens of tuning parameters. There is growing feeling in oceanographic community that new type of physically justified models needs to be developed.

The step in that direction has been done through the development of the alternative ZRP [34, 27] approach to the formulation of balanced source terms for wave generation in HE. Contrary to the previous attempts of building the detailed-balance source terms, it is neither based on the development of a rigorous analytic theory of turbulent atmospheric boundary layer, nor on reliable and repeatable air to ocean momentum measurements. It is constructed in the artificial way, realizing, in a sense, "the poor man approach", based on the finding of two-parameter family of HE self-similar solutions and its restriction to the single-parameter one via comparison with the data of multiple field experimental observations. This ZRP self-similarity analysis is summarized in the following dependencies:

$$\epsilon = \chi^{p+q} F(\omega \chi^q) \tag{6}$$

$$10q - 2p = 1, \quad q = \frac{1}{2+s} \tag{7}$$

$$p = 1, \quad q = 3/10, \quad s = 4/3 \tag{8}$$

$$E(\chi) = E_0 \chi^p \tag{9}$$

$$< \omega(\chi) >= \omega_0 \chi^{-q} \tag{10}$$

where $E(\chi)$ and $< \omega(\chi) >$ are the total wave energy and the mean frequency as the functions of the dimensionless fetch coordinate $\chi = xg/U^2$, where x is the dimensional fetch coordinate in meters, g is the gravity acceleration and U is the wind speed; $s = 4/3$ is the index of power-like wind forcing dependency on frequency $\sim \omega^s$ of ZRP wind source term (see Eq.(13) for details); E_0 and ω_0 are the constants.

In the following chapters we numerically compare ZRP model [34, 27] with the MD1 and MD2 models. MD1 model is based on the set of the forcing and dissipation source functions, described in [7]. MD2 model is the "synthetic" model, carrying the details of ZRP as wells as MD1 model.

One should emphasize that ZRP and MD1 source terms sets assume different underlying physics: ZRP model assumes the leading role of the nonlinear interaction term and wave energy cascade from spectral peak energy input area to the energy dissipation region of high wave numbers, while MD1, as show our numerical experiments, dissipates most of the wave energy at the intermediate wave numbers closer to the spectral peak. That results in significant differences in total wave energy and mean frequency behavior along the fetch as well as the details of wave energy spectral distributions.

The numerical experiments performed with the "synthetic" MD2 model showed the improvement of MD1 model self-similar properties and wave energy spectral characteristics, arguing in favor of high-frequency wave energy dissipation mechanism in HE.

The following chapters describe the details of studied models and present the supporting facts to the explained point of view.

2. The models formulation and numerical approach

The numerical simulation was based on the solution of stationary version of the Eq.(1) in limited fetch approximation $\frac{\partial \varepsilon}{\partial t} = 0$:

$$\frac{1}{2} \frac{g \cos\theta}{\omega} \frac{\partial \epsilon}{\partial x} = S_{nl} + S_{wind} + S_{diss} \tag{11}$$

where $\vec{x}$ is the coordinate axis orthogonal to the shore and θ is the angle between individual wavenumber $\vec{k}$ and the direction of $\vec{x}$.

The stationarity in Eq.(11) is somewhat difficult for numerical simulation, since it contains the singularity in the form of $\cos\theta$ in front of $\frac{\partial \epsilon}{\partial x}$. This problem was overcome by zeroing out of one half of the Fourier space of the system for the waves propagating backward to the shore. Since the energy of the waves against the wind is small with respect to waves propagating in the offshore direction, such an approximation is quite reasonable for our purposes.

All simulations used WRT (Webb-Resio-Tracy) method [25], which calculates the nonlinear interaction term in the exact form. The presented numerical simulation utilized the version of WRT method, previously used in [26, 18, 14, 16, 20, 13, 12, 3, 17, 27, 4], on the grid of 71 logarithmically spaced points in the frequency range from 0.1 Hz to 2.0 Hz and 36 equidistant points in the angle domain from 0 to 2π. The constant space step in the range from 1 m to 2 m has been used for explicit first order accuracy integration in fetch coordinate.

All numerical simulations discussed in the current paper have been started from uniform noise energy distribution in Fourier space $\varepsilon(\omega,\theta) = 10^{-6}\ \ m^4$, corresponding to small initial wave height with effectively negligible nonlinearity level. The constant wind speed 10 m/sec was assumed blowing away from the shore line, along the fetch. The assumption of the constant wind speed is a necessary simplification, due to the fact that ZRP numerical simulation was compared to various field experiments, and the considered set-up is the simplest physical situation, which can be modeled and realized in nature.

2.1. ZRP model

ZRP wind input term has been used in the form [34, 17, 27]

$$S_{in}^{ZRP}(\omega,\theta) = \gamma(\omega,\theta)\cdot\varepsilon(\omega,\theta) \tag{12}$$

$$\gamma(\omega,\theta) = \begin{cases} 0.05\frac{\rho_a}{\rho_w}\omega\left(\frac{\omega}{\omega_0}\right)^{4/3} q(\theta) \ \text{ for } f_{min}\le f\le f_d, \ \ \omega = 2\pi f \\ 0 \ \text{ otherwise} \end{cases} \tag{13}$$

$$q(\theta) = \begin{cases} \cos 2\theta \ \text{ for } -\pi/4\le\theta\le\pi/4 \\ 0 \ \text{ otherwise} \end{cases} \tag{14}$$

$$\omega_0 = \frac{g}{U}, \ \ \frac{\rho_a}{\rho_w} = 1.3\cdot 10^{-3} \tag{15}$$

where $U = 10$ m/sec is the wind speed at the reference level of 10 meters, ρ_a and ρ_w are the air and water density correspondingly. Frequencies $f_{min} = 0.1$ Hz and $f_d = 1.1$ Hz have been used.

The ZRP model source functions set is accomplished with the "implicit dissipation" term S_{diss} playing dual role of direct energy cascade flux sink due to wave breaking as well as numerical scheme stabilization factor at high wave-numbers. It is made via continuation of the spectrum from ω_d by Phillips law $A(\omega_d)\cdot\omega^{-5}$ [15], decaying faster than equilibrium spectrum ω^{-4}, and providing high-frequency wave energy dissipation. The corresponding analytic parameterization of this dissipation term is not determined, while is not in principle impossible to figure out in some way.

The coefficient $A(\omega_d)$ in front of ω^{-5} is unknown, but is not required to be defined in an explicit form. Instead, it is dynamically determined from the continuity condition of the spectrum, at frequency ω_d, on every time step. In other words, the starting point of the Phillips spectrum coincides with the last frequency point of the dynamically changing spectrum, at $\omega_d = 2\pi f_d$, where $f_d \simeq 1.1\ Hz$, as per [13]. This is the way the high frequency "implicit" damping is incorporated into ZRP model.

2.2. MD1 model

The MD1 model [7] is briefly formulated below in relation to the studied deep water case in the absence of average current.

For reader convenience, we briefly reformulate it in here. The wind source function is

$$S_{in}^{MD} = A_1(U_{\lambda/2}\cos\theta - c)|U_{\lambda/2}\cos\theta - c|\frac{k\omega}{g}\frac{\rho_a}{\rho_w}\varepsilon(k,\theta) \tag{16}$$

where θ is the angle between wind direction and waves with the wavenumber k, $A_1 = 0.11$ is the sheltering coefficient, $U_{\lambda/2}$ is the wind speed at one half wavelength above the surface for logarithmic profile

$$U_{\lambda/2} = \frac{U_*}{\kappa}\ln\frac{z}{z_0} \tag{17}$$

where U_* is the friction velocity, $\kappa = 0.41$ - Von Karman constant, $z = \frac{1}{2}\lambda$ is the elevation equal to a fixed fraction $\frac{1}{2}$ of the spectral peak wavelength $\lambda = 2\pi/k_p$ (k_p is the wavenumber of the spectral peak) and $z_0 = \alpha_C u_*^2/g$ is the surface roughness subject to Charnock constant $\alpha_C = 0.015$ ([6]).

The dissipation source function is the "spilling breakers" dissipation function [7]

$$S_{sb}^{MD1} = -A_2 \left[1 + A_3 MS\,M^2(k,\theta)\right]^2 [B(k,\theta)]^{2.53}\,\omega(k)\varepsilon(k,\theta) \tag{18}$$

where

$$MS\,M^2(k,\theta) = \int_0^k p^2 \varepsilon(p,\theta) dp \tag{19}$$

is the Mean Square Slope (MSS) in the direction θ of all waves longer than $\frac{2\pi}{k}$, $B(k,\theta) = k^4\varepsilon(k,\theta)$ is the degree of saturation, $A_2 = 46.665$, $A_3 = 240$.

Due to fast growing factor $\omega^{21.24}$ in the Eq.(18), the numerical solution of MD1 model is prone to numerical instabilities, if the dissipation source function is used in a straightforward way as the part of "overall" right-hand side source function, especially due to inability of significantly splitting the characteristic space integration step ~ 1 m for acceptable simulation times. In this case, the different treatment of the nonlinear dissipation Eq.(18) is useful – one can analytically solve the dissipation part of HE

$$\frac{1}{2}\frac{g\cos\theta}{\omega}\frac{\partial\varepsilon}{\partial x} = S_{sb}^{MD} \tag{20}$$

on every space integration step h in the adiabatic approximation, assuming that MMS change is slower than wave energy density ε for every space step h.

$$\varepsilon_{n+1} = \varepsilon_n \Big/ \left[1 + 2.52 A_2 \left[1 + MS\,M^2\right]^2 \frac{2\omega}{g\cos\theta} h\varepsilon_n^{2.53}\right]^{1/2.53} \tag{21}$$

where n is the numerical integration step number and h is the numerical discretisation step along the fetch. Such treatment of the dissipation function provides relatively instability-free integration technique.

2.3. MD2 model

The MD2 model was created to check the influence of the nonlinear dissipation Eq.(18), through MD1 model modification via keeping the wind source function Eq.(16) with angle and frequency restrictions of Eqs.(13)-(14), but replacing the nonlinear dissipation by the "implicit" dissipation function, described in the subsection 2.1

In other words, the MD2 model is similar to ZRP model up to the substitution of Eq.(12) by Eq.(16).

3. Numerical results

Figure 1 presents the total wave energy as the function of the fetch coordinate for ZRP, MD1 and MD2 models. One should keep in a mind that ZRP curve is consistent with self-similar solution Eq.(6) with the index $p = 1$, reproduces the data of more than a dozen of field observations, analyzed in [1], and can be used, therefore, as the benchmark function.

The corresponding values of indices p for ZRP, MD1 and MD2 models along the fetch are presented on Figure 2. While ZRP model exhibits asymptotic convergence to the self-similar index target value $p = 1$, MD1 model does not. MD2 model does it as well, but to the different index value $p \simeq 0.5$ with somewhat slower convergence. That observation demonstrates self-similar behavior in ZRP and MD2 models. One should note fairly good correspondence between ZRP and MD1 models for wave energy growth on Figure 1 for "practical" dimensional fetches up to ~ 20 km, which justifies MD1 tuning quality against the total energy growth.

The Figure 3 shows the consistency between all three models for the average frequency behavior in the range of 25% scatter for far enough dimensional fetches exceeding 20 km.

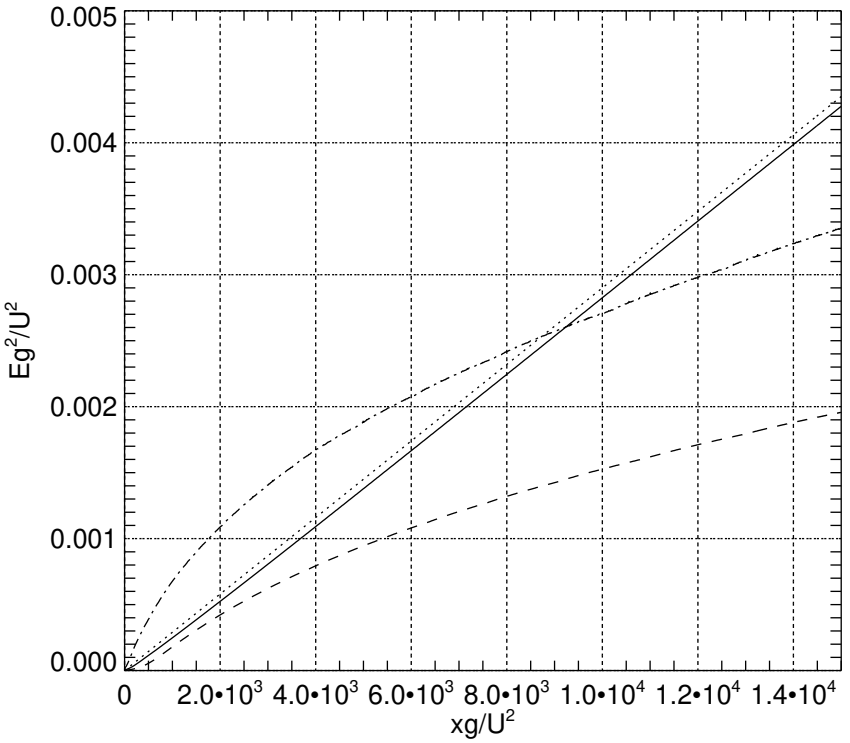

Fig. 1. Dimensionless energy Eg^2/U^4 versus dimensionless fetch xg/U^2 for wind speed $U = 10$ m/sec limited fetch case. Solid line - ZRP case, dotted line - self-similar solution with the empirical coefficient in front of it: $2.9 \cdot 10^{-7} xg/U^2$; dashed line - MD1 case; dash-dotted line - MD2 case.

ZRP model, as seen from Figure 4, demonstrates the behavior consistent with the self-similar dependence Eq.(10) with asymptotic convergence to the target self-similar index value $q = 0.3$, while MD1 and MD2 models show somewhat slower convergence to the different value of self-similar index $q \simeq 0.2$.

The oscillations observed in the behavior of index q could be attributed to the finite grid resolution used in the simulation, since the narrow spectral peak moves continuously between discrete frequencies in a manner that cannot be matched in these discretized simulations.

The check of calculated magic number $(10q - 2p)$ (see Eq.(7)) is presented on Figure 5. It exhibits asymptotic convergence of ZRP model to the target value of 1, while MD1 and MD2 models converge to the slightly lower values $0.8 \div 0.9$ somewhat slower along the fetch.

The nature of oscillation, especially obvious in MD1 and MD2 cases is attributed to the grid discreteness effects, described above.

Fig.6 presents angle-integrated wave energy spectrum for ZRP case, as the function of frequency, in logarithmic coordinates, for the dimensional fetch coordinate $x \simeq 20$ km. One can see that it consists of the segments of:

- the spectral peak region
- the inertial (equilibrium) range ω^{-4} spanning from the spectral peak to the beginning of the "implicit dissipation" $f_d = 1.1$ Hz
- Phillips high frequency tail ω^{-5} starting approximately from $f_d = 1.1$ Hz

Figure 7 presents decimal logarithm of angle-integrated energy spectrum for MD1 case, as the function of decimal logarithm of frequency for the dimensional fetch coordinate $x \simeq 20$ km. One can note that neither portion of the spectral tail to the right of the spectral peak can be approximated by $\sim \omega^{-4}$, or $\sim \omega^{-5}$ spectra. The only portion of the wave energy spectrum, which could be approximated by power-like function, is the region of high frequencies

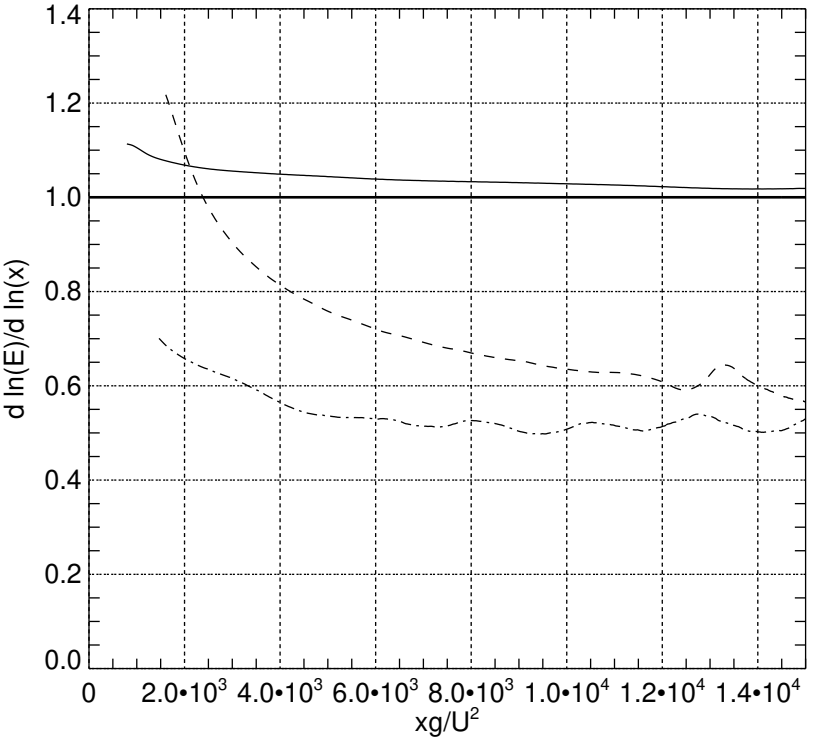

Fig. 2. Energy local power function index $p = \frac{d \ln E}{d \ln x}$ as the function of dimensionless fetch xg/U^2 for wind speed $U = 10$ m/sec fetch limited case. Theoretical value of self-similar index $p = 1$ - thick horizontal solid line. Solid line - ZRP case; dashed line - MD1 case; dash-dotted line - MD2 case.

$f > 1.1$ Hz with $\sim \omega^{-8.4}$ spectral shape. That sort of fast decaying spectra, however, was never observed in the field experiments, to the best of the author knowledge.

Figure 8 presents decimal logarithm of angle-integrated energy spectrum for MD1 case, as the function of frequency, for dimensional fetch coordinate $x \simeq 20$ km. One can see that the portion of the spectrum, for the frequencies range from 0.5 Hz to 1.2 Hz, can be approximated by the function $\sim 10^{-3.3f}$, which is unknown for experimental field observations either.

Appearance of both exponential and power-like spectra for intermediate and high frequency ranges correspondingly, finds its explanation from Figure 9. It shows that significant part of the wave breaking dissipation is localized in the area of intermediate frequencies, right adjacent to the spectral peak area. Such localization of the wave-breaking dissipation causes exponential decay at the intermediate frequencies of the spectral tail.

Fig.10 presents angle-integrated energy spectrum for MD2 case, as the function of the frequency, in logarithmic coordinates, for the dimensional fetch coordinate $x \simeq 20$ km. One can see that, just like in ZRP case, it consists of the segments of:

- the spectral peak region
- the inertial (equilibrium) range ω^{-4} spanning from the spectral peak to the beginning of the "implicit dissipation" $f_d = 1.1$ Hz
- Phillips high frequency tail ω^{-5} starting approximately from $f_d = 1.1$ Hz

That observation is the evidence of domination of nonlinear quadruplet interaction term, exhibiting KZ solution in the inertial range of frequencies from the spectral peak area to $f_d = 1.1$ Hz.

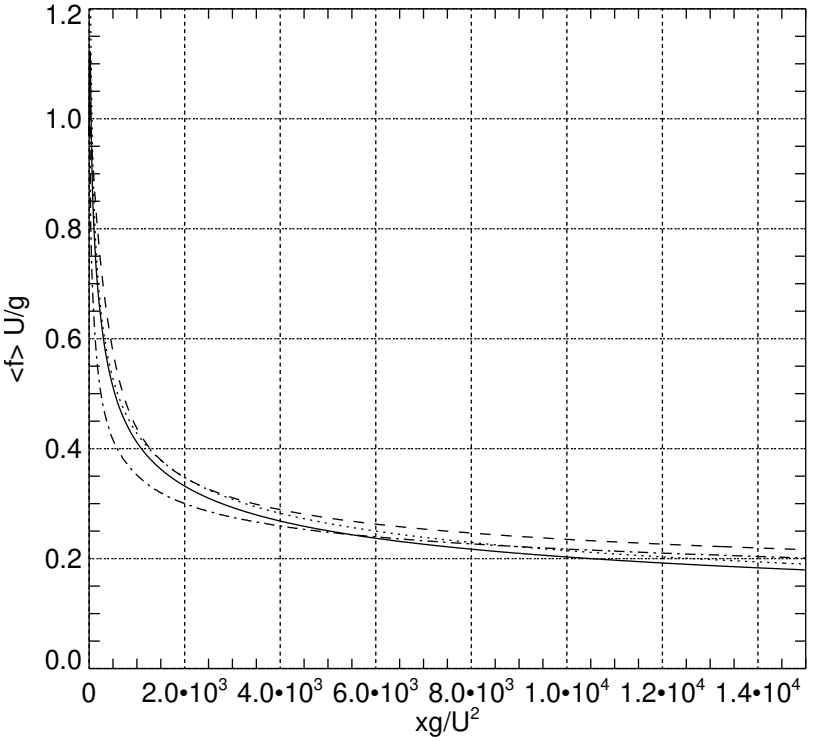

Fig. 3. Dimensionless mean frequency, as the function of the dimensionless fetch, calculated as $< f >= \frac{1}{2\pi}\frac{\int \omega n d\omega d\theta}{\int n d\omega d\theta}$, where $n(\omega,\theta) = \frac{\varepsilon(\omega,\theta)}{\omega}$ is the wave action spectrum, for wind speed 10 m/sec (solid line). The dash-dotted line is the self-similar dependence $3.4 \cdot \left(\frac{xg}{U^2}\right)^{-0.3}$ with the empirical coefficient in front of it; dashed line - MD1 case; dash-dotted line - MD2 case.

4. Conclusions

We analyzed numerically recently developed models for balanced source terms in HE for fetch-limited wind wave growth. These models utilize different techniques: ZRP model studies the family of analytical solutions of HE, restricting them through the experimental observations, while MD1 model utilizes mostly experimental techniques for their formulation. We also studied the "synthetic" approach - MD2 model - incorporating the features from ZRP as well as MD1 models.

The results of numerical simulation show that there is the significant difference between ZRP and MD1 models. While ZRP model exhibits self-similar properties, MD1 model shows only some of them with slower asymptotic convergence. As far as concerns Fourier space of the wave energy spectra, ZRP and MD2 models exhibit KZ spectrum, while MD1 model exhibit exponentially decaying spectral tail in the intermediate wave numbers. It is caused by different localization of the wave energy absorption: while ZRP approach relies of high-frequency dissipation, MD1 model utilizes intermediate wave numbers wave energy absorption. Besides that facts, ZRP model reproduces the wave energy and mean frequency behavior of more than a dozen of field experimental observation.

It is quite fascinating that MD2 "synthetic" model improves the self-similar properties of MD1, such as wave energy, average frequency indices, "magic numbers" as well as spectral characteristics of the angle-averaged spectra, such as $\sim \omega^{-4}$ spectral tails. This observation, in our view, emphasizes the fact that replacement of fairly complex nonlinear wave-breaking dissipation term by simple "implicit" dissipation in the form of Phillips tail could improve the quality of MD1 model under condition of re-tuning of wind wave energy input sheltering coefficient.

The presented research shows that relatively wide class of source terms, used in conjunction with exact nonlinear term S_{nl} and "implicit" high-frequency dissipation, can exhibit consistency with predicted self-similar properties of HE, KZ wave energy spectral shapes and data of the experimental observations.

The authors hope that this research will offer additional guidance for creation of tuning-free operational models .

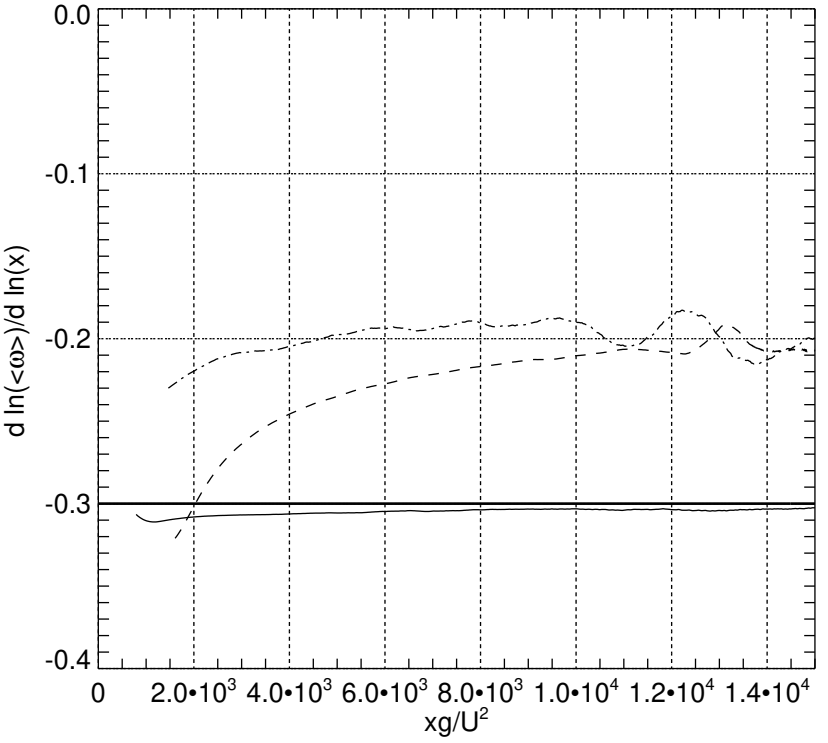

Fig. 4. Local mean frequency exponent $-q = \frac{d \ln <\omega>}{d \ln x}$ as the function of dimensionless fetch xg/U^2 for $U = 10$ m/sec limited fetch case. ZRP case - solid line; dashed line - MD1 case; dash-dotted line - MD2 case. Thick horizontal solid line - target value of the self-similar exponent $q = 0.3$.

5. Acknowledgments

The research presented in the section 3 has been accomplished due to the support of the grant Wave turbulence: the theory, mathematical modeling and experiment of the Russian Scientific Foundation No 14-22-00174. The research set forth in the section 1, was funded by the program of the presidium of RAS "Nonlinear dynamics: fundamental problems and applications".

The authors gratefully acknowledge the support of these foundations.

References

1. Badulin, S., Babanin, A.V., Resio, D.T., Zakharov, V., 2007. Weakly turbulent laws of wind-wave growth. J.Fluid Mech. 591, 339 – 378.
2. Badulin, S.I., Pushkarev, A.N., D.Resio, Zakharov, V.E., 2005. Self-similarity of wind-driven sea. Nonlinear Proc. in Geophysics 12, 891 – 945.
3. Badulin, S.I., Zakharov, V.E., 2012. The generalized Phillips' spectra and new dissipation function for wind-driven seas. arXiv:1212.0963 [physics.ao-ph] , 1 – 16.
4. Badulin, S.I., Zakharov, V.E., 2017. Ocean swell within the kinetic equation for water waves. Nonlinear Processes in Geophysics 24, 237–253. URL: https://www.nonlin-processes-geophys.net/24/237/2017/, doi:10.5194/npg-24-237-2017.
5. Cavaleri, L., Alves, J.H., Ardhuin, F., Babanin, A., Banner, M., Belibassakis, K., Benoit, M., Donelan, M., Groeneweg, J., Herbers, T., Hwang, P., Janssen, P., Janssen, T., Lavrenov, I., Magne, R., Monbaliu, J., Onorato, M., Polnikov, V., Resio, D., Rogers, W., Sheremet, A., Smith, J.M., Tolman, H., van Vledder, G., Wolf, J., Young, I., 2007. Wave modelling the state of the art. Progress in Oceanography 75, 603 – 674. doi:https://doi.org/10.1016/j.pocean.2007.05.005.
6. Charnock, H., 1955. Wind stress on a water surface. Q.J.R. Meteorol. Soc. 81, 639 – 640.
7. Donelan, M.A., Curcic, M., Chen, S.S., Magnusson, A.K., 2012. Modeling waves and wind stress. Journal of Geophysical Research: Oceans 117, n/a–n/a. URL: http://dx.doi.org/10.1029/2011JC007787, doi:10.1029/2011JC007787. c00J23.
8. Dyachenko, A.I., Kachulin, D.I., Zakharov, V.E., 2015. Evolution of one-dimensional wind-driven sea spectra. JETP Letters 102, 577 – 581.
9. Gagnaire-Renou, E., Benoit, M., Badulin, S., 2011. On weakly turbulent scaling of wind sea in simulations of fetch-limited growth. Journal of Fluid Mechanics 669, 178–213. doi:10.1017/S0022112010004921.

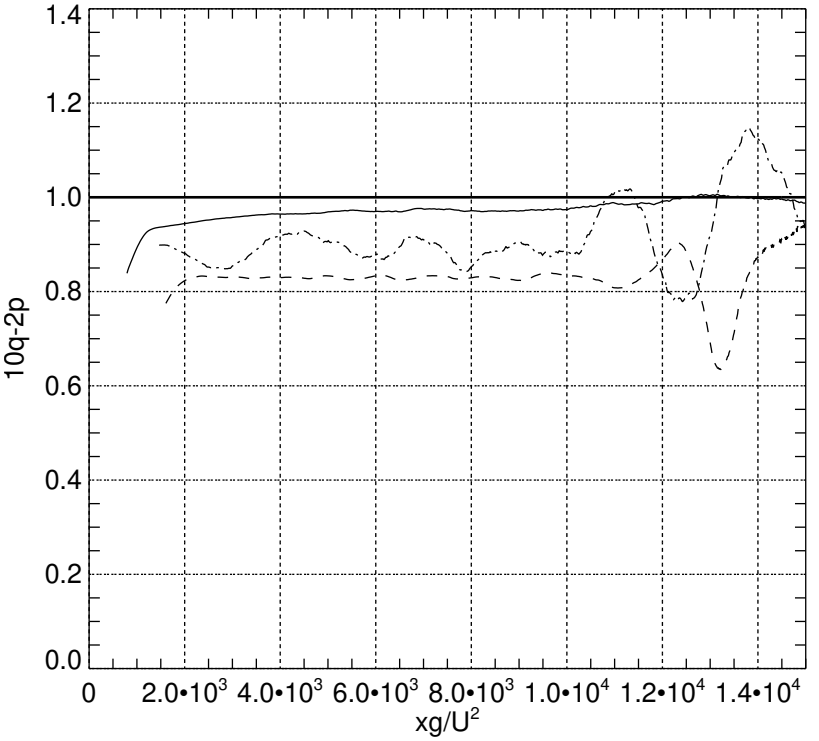

Fig. 5. "Magic number" $10q - 2p$ as a function of dimensionless fetch xg/U^2 for wind speed $U = 10$ m/sec limited fetch case. ZRP case - solid line; dashed line - MD1 case; dash-dotted line - MD2 case. Thick horizontal solid line - self-similar target value $10q - 2p = 1$.

10.Hasselmann, K., 1962. On the non-linear energy transfer in a gravity-wave spectrum. Part 1. General theory. Journal of Fluid Mechanics 12, 481 – 500.
11.Hasselmann, K., 1963. On the non-linear energy transfer in a gravity wave spectrum. Part 2. Conservation theorems; wave-particle analogy; irrevesibility. Journal of Fluid Mechanics 15, 273 – 281.
12.Korotkevich, A.O., Pushkarev, A.N., Resio, D., Zakharov, V.E., 2008. Numerical verification of the weak turbulent model for swell evolution. Eur. J. Mech. B - Fluids 27, 361 – 387.
13.Long, C., Resio, D., 2007. Wind wave spectral observations in Currituck Sound, North Carolina. JGR 112, C05001.
14.Perrie, W., Zakharov, V.E., 1999. The equilibrium range cascades of wind-generated waves. Eur. J. Mech. B/Fluids 18, 365 – 371.
15.Phillips, O.M., 1966. The dynamics of the upper ocean. Cambridge monographs on mechanics and applied mathematics, Cambridge U.P.
16.Pushkarev, A., Resio, D., Zakharov, V., 2003. Weak turbulent approach to the wind-generated gravity sea waves. Physica D 184, 29 – 63.
17.Pushkarev, A., Zakharov, V., 2016. Limited fetch revisited: comparison of wind input terms, in surface wave modeling. Ocean Modeling 103, 18 – 37. doi:10.1016/j.ocemod.2016.03.005.
18.Resio, D., Perrie, W., 1989. Implications of an f^{-4} equilibrium range for wind-generated waves. JPO 19, 193 – 204.
19.Resio, D.T., Long, C.E., 2007. Wind wave spectral observations in Currituck Sound, North Carolina. J. Geophys. Res. 112, C05001.
20.Resio, D.T., Long, C.E., Vincent, C.L., 2004. Equilibrium-range constant in wind-generated wave spectra. J. Geophys. Res. 109, CO1018.
21.Resio, D.T., Perrie, W., 1991. A numerical study of nonlinear energy fluxes due to wave-wave interactions in a wave spectrum. Part I: Methodology and basic results. J. Fluid Mech. 223, 603 – 629.
22.SWAN, 2015. `http://swanmodel.sourceforge.net/`.
23.Toba, Y., 1972. Local balance in the air-sea boundary processes. pt. 1: On the growth process of wind waves. J. Oceanogr. Soc. Japan. 28, 109 – 121.
24.Tolman, H.L., 2013. User manual and system documentation of WAVEWATCH III. Environmental Modeling Center, Marine Modeling and Analysis Branch .
25.Tracy, B., Resio, D., 1982. Theory and calculation of the nonlinear energy transfer between sea waves in deep water. WES report 11, U.S. Army Engineer Waterways Experiment Station, Vicksburg, MS.
26.Webb, D.J., 1978. Non-linear transfers between sea waves. Deep-Sea Res. 25, 279 – 298.
27.Zakharov, V., Resio, D., Pushkarev, A., 2017. Balanced source terms for wave generation within the hasselmann equation. Nonlin. Processes Geophys. 24, 581 – 597. doi:https://doi.org/10.5194/npg-24-581-2017.
28.Zakharov, V.E., 2010. Energy balances in a wind-driven sea. Physica Scripta T142, 014052.
29.Zakharov, V.E., Badulin, S.I., 2011. On energy balance in wind-driven sea. Doklady Akademii Nauk 440, 691 – 695.

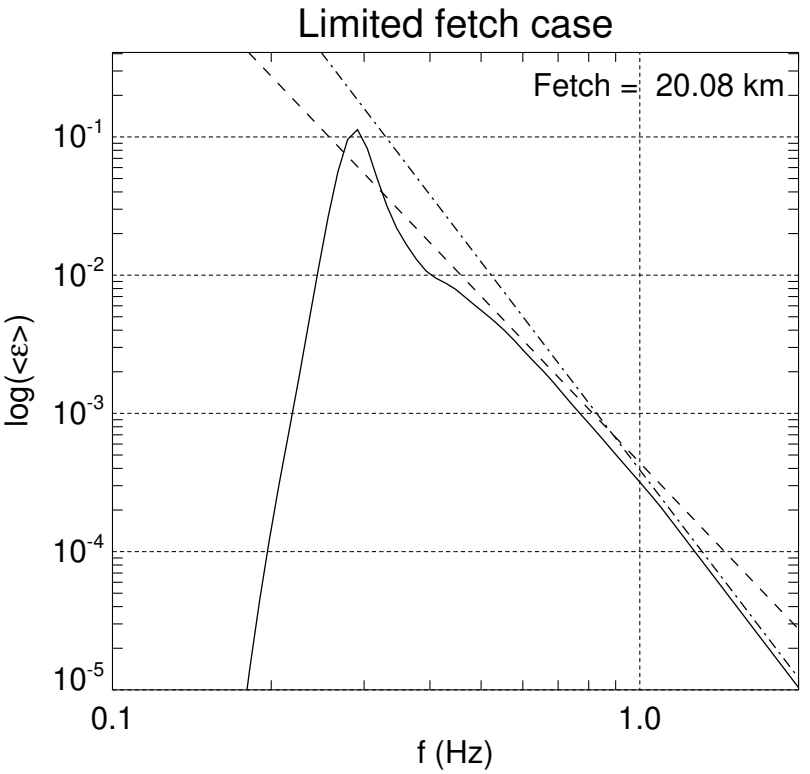

Fig. 6. Decimal logarithm of the angle averaged spectrum as the function of the decimal logarithm of the frequency for wind speed $U = 10$ m/sec fetch limited ZRP case - solid line. Spectrum $\sim f^{-4}$ - dashed line, spectrum $\sim f^{-5}$ - dash-dotted line.

30.Zakharov, V.E., Filonenko, N.N., 1966. The energy spectrum for stochastic oscillation of a fluid's surface. Dokl.Akad.Nauk. 170, 1992 – 1995.
31.Zakharov, V.E., Filonenko, N.N., 1967. The energy spectrum for stochastic oscillations of a fluid surface. Sov. Phys. Docl. 11, 881 – 884.
32.Zakharov, V.E., Korotkevich, A.O., Prokofiev, A.O., 2009. On dissipation function of ocean waves due to whitecapping, in: Simos, T.E., G.Psihoyios, Tsitouras, C. (Eds.), American Institute of Physics Conference Series, pp. 1229 – 1237.
33.Zakharov, V.E., L'vov, V.S., Falkovich, G., 1992. Kolmogorov Spectra of Turbulence I: Wave Turbulence. Springer-Verlag.
34.Zakharov, V.E., Resio, D., Pushkarev, A., 2012. New wind input term consistent with experimental, theoretical and numerical considerations. http://arxiv.org/abs/1212.1069/.

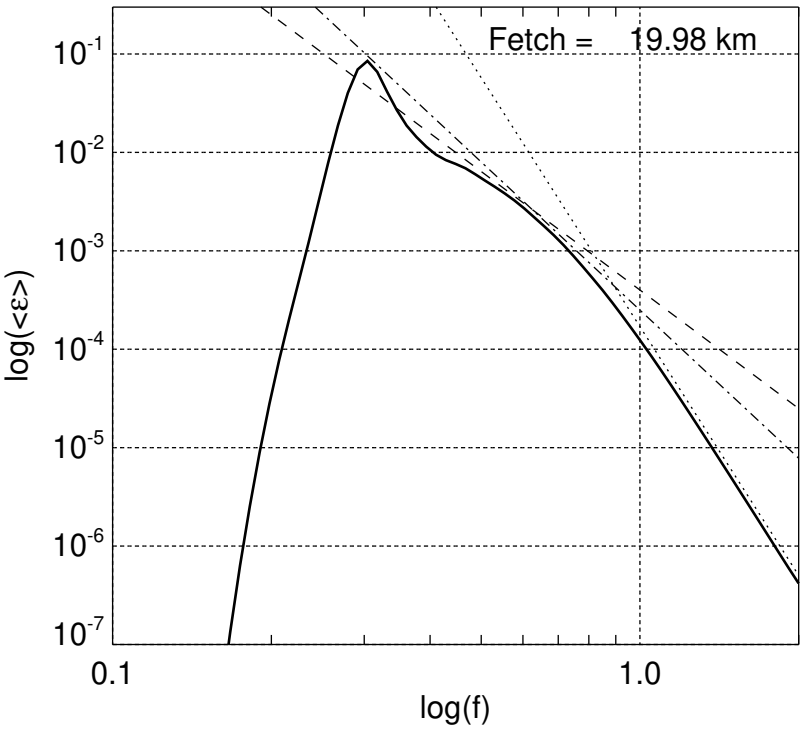

Fig. 7. Decimal logarithm of the angle averaged spectrum as the function of the decimal logarithm of the frequency for wind speed $U = 10$ m/sec limited fetch MD1 case - solid line. Spectrum $\sim f^{-4}$ - dashed line, spectrum $\sim f^{-5}$ - dash-dotted line.

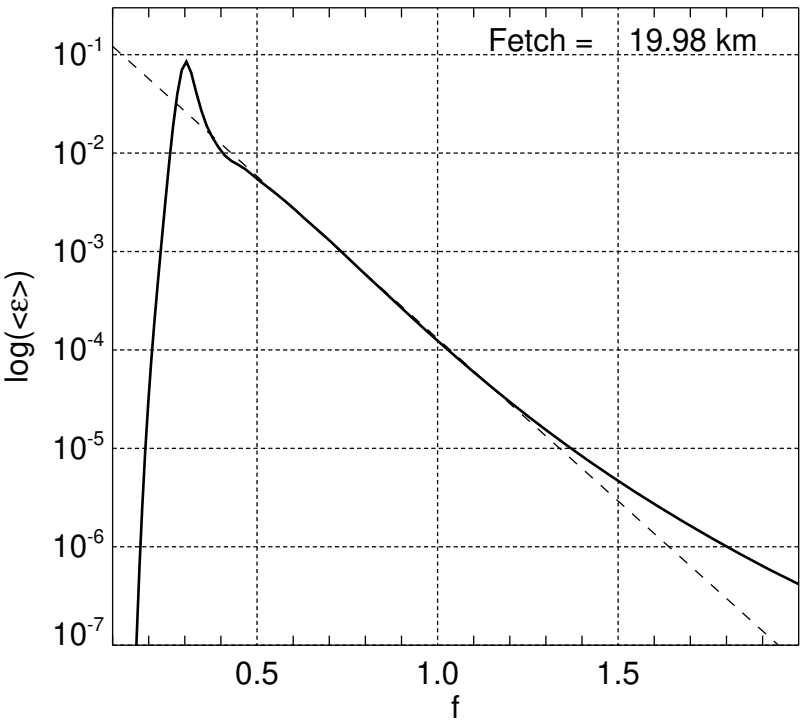

Fig. 8. Decimal logarithm of the angle averaged spectrum as the function of the frequency for wind speed $U = 10$ m/sec limited fetch MD1 case - solid line. Spectrum $\sim 10^{-3.3f}$ - dashed line.

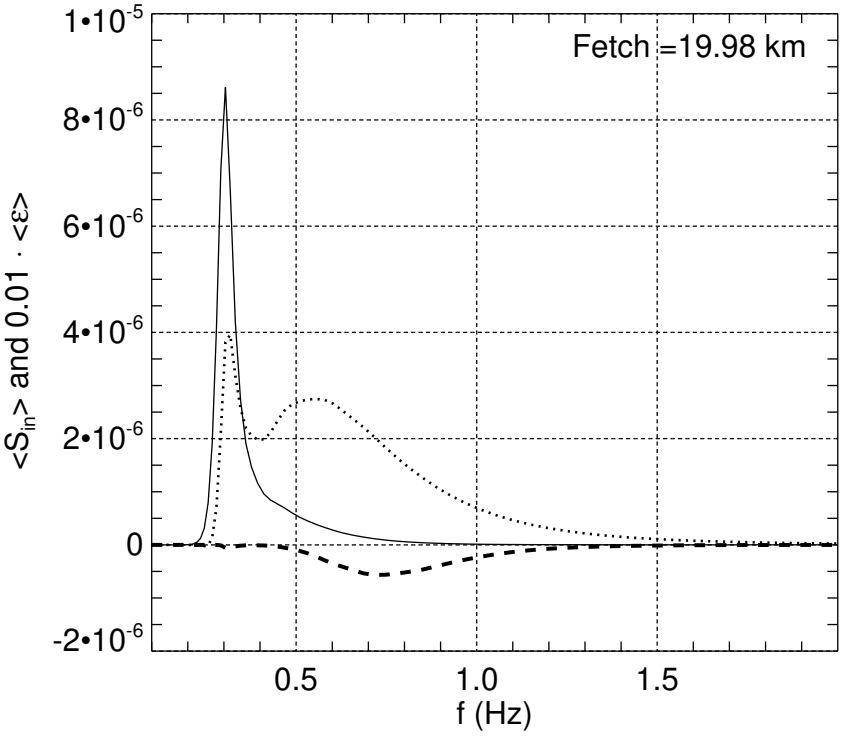

Fig. 9. Angle averaged wave energy wind input $< S_{in} >= \frac{1}{2\pi}\int \gamma_{in}(\omega,\theta)\varepsilon(\omega,\theta)d\theta$ (dotted line), wave braking dissipation $< S_{diss} >= \frac{1}{2\pi}\int \gamma_{diss}(\omega,\theta)\varepsilon(\omega,\theta)d\theta$ (dashed line) and angle averaged spectrum $< \varepsilon >= \frac{1}{2\pi}\int \varepsilon(\omega,\theta)d\theta$ (solid line) as the functions of the frequency f (solid line).

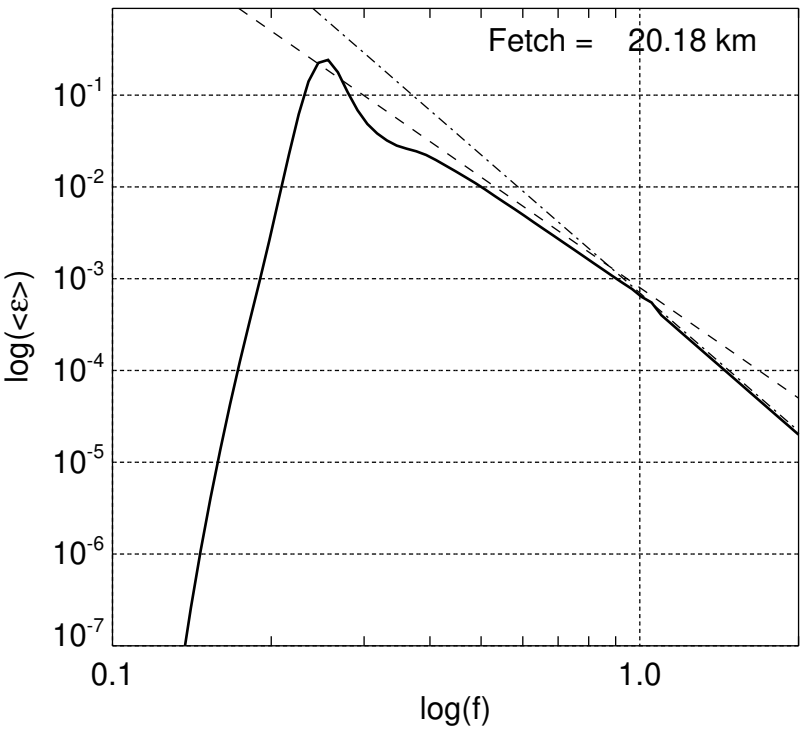

Fig. 10. Decimal logarithm of the angle averaged spectrum as the function of the decimal logarithm of the frequency for wind speed U = 10 m/sec limited fetch MD2 case - solid line. Spectrum $\sim f^{-4}$ - dashed line, spectrum $\sim f^{-5}$ - dash-dotted line.